

Bayesian 3D tracking from monocular video

Ernesto Brau[†]

ernesto@cs.arizona.edu

Jinyan Guan[†]

jguan1@email.arizona.edu

Kyle Simek[†]

ksimek@email.arizona.edu

Luca Del Pero^{*}

ldelper@inf.ed.ac.uk

Colin Reimer Dawson[‡]

cdawson@email.arizona.edu

Kobus Barnard[‡]

kobus@sista.arizona.edu

[†]Computer Science
University of Arizona

[‡]School of Information
University of Arizona

^{*}School of Informatics
University of Edinburgh

Abstract

We develop a Bayesian modeling approach for tracking people in 3D from monocular video with unknown cameras. Modeling in 3D provides natural explanations for occlusions and smoothness discontinuities that result from projection, and allows priors on velocity and smoothness to be grounded in physical quantities: meters and seconds vs. pixels and frames. We pose the problem in the context of data association, in which observations are assigned to tracks. A correct application of Bayesian inference to multi-target tracking must address the fact that the model's dimension changes as tracks are added or removed, and thus, posterior densities of different hypotheses are not comparable. We address this by marginalizing out the trajectory parameters so the resulting posterior over data associations has constant dimension. This is made tractable by using (a) Gaussian process priors for smooth trajectories and (b) approximately Gaussian likelihood functions. Our approach provides a principled method for incorporating multiple sources of evidence; we present results using both optical flow and object detector outputs. Results are comparable to recent work on 3D tracking and, unlike others, our method requires no pre-calibrated cameras.

1. Introduction

Tracking remains difficult when there are multiple targets interacting and occluding each other. These difficulties are common in many applications such as surveillance, mining video data, and video retrieval, motivating much recent work in multi-object tracking [39, 4, 5, 23, 24, 6, 41]. In these contexts, it often makes sense to analyze extended frame sequences (“off-line” tracking), and the camera parameters are often unknown.

In this paper we develop a fully 3D Bayesian approach

for tracking an unknown and changing number of people in a scene using video taken from a single, fixed viewpoint. We propose a generative statistical model that provides the distribution of data (evidence) given an association, where we extend the well-known formulation of Oh et al. [31]. We model people as elliptical right-angled cylinders moving on a relatively horizontal ground plane. We infer camera parameters and people's sizes as part of the tracking process. Further, with a reasonable value for the mean height of people, we can establish location with respect to the camera in absolute units (i.e., meters).

This formulation enables inference in the constant dimension data-association space, provided that we integrate out the continuous model parameters such as those associated with trajectories. In other words, we estimate the marginal likelihoods during inference, which deals with potential dimensionality issues due to an unknown number of tracks. This principled approach is very amenable to extensions, such the incorporation of new model elements (e.g., pose estimation and gaze direction) or new sources of evidence (e.g., color and texture).

Given a model hypothesis, we project each person cylinder into each frame using the current camera, computing their visibility as a consequence of any existing occlusion. We then evaluate the hypothesis using evidence from the output of person detectors and optical flow. Our method thus integrates tracking as detection (e.g., [32, 23, 1]) and classical approaches like tracking as following evidence locally in time as is common in filtering methods (e.g., [20, 22]). We use a Gaussian process in world coordinates to provide a smoothness prior on motion with respect to absolute measures. Given a reasonable kernel, observations that are far apart in time do not influence each other much, and we exploit this for efficiency.

To track multiple people in videos we infer an association between persons and detections, collaterally determin-

ing a likely set of 3D trajectories for the people in the scene. We use MCMC sampling (§3) to sample over associations, and, for a given association, we then sample trajectories to search for a probable one, conditioned on the association. We use this to estimate the integral over all trajectories, again conditioned on the association. During inference we also sample the global parameters for the video which includes the camera and the false detection rate, which we consider to be a function of the scene background.

Closely related work. Our data association approach extends that of Oh et al. [31]. We further follow Brau et al. [8] who used Gaussian processes for trajectory smoothness while searching over associations by sampling. Others [40, 7] use a similar data association model, but propose an effective non-sampling approach for inference. All these efforts are focused on association of points alone; neither appearance or geometry are considered.

With respect to representation, several others share our preference for 3D Bayesian models for humans (e.g., [36, 11, 37, 9]). In particular, Isard and MacCormick [21] use a 3D cylinder model for multi-person tracking using a single, known camera. However, this approach does not deal with data association, since it is not detection-based. Similarly, there is other work in tracking objects on the 3D ground plane [16, 13, 28] without considering data association. Other approaches estimate data association as well as model parameters [39, 19, 10]. However, we model data association explicitly in a generative way, as opposed to estimating it as a by-product of inference. In addition, none of these approaches model humans as 3D objects.

Andriyenko and Schindler [3] pose data association as an integer linear program. In subsequent work [4], they formulate an energy approach for multi-target tracking in 3D that includes terms for image evidence, physics based priors, and a simplicity term that pushes towards fewer trajectories. Later, Andriyenko et al. [5] attempt to solve both data association and trajectory estimation problems using similar modeling ideas as in their previous work. In contrast to our work, they simultaneously optimize both association and trajectory energy functions, which results in a space of varying dimensionality.

Technical contributions include: (1) A full Bayesian formulation that incorporates both data association and the 3D geometry of the scene; (2) Robust inference of camera parameters while tracking; (3) A Gaussian process prior on trajectory smoothness applied in absolute 3D coordinates; (4) Inferring people’s heights and widths simultaneously while tracking to improve performance; (5) Explicitly handling occlusion as a natural consequence of perspective projection while tracking; (6) Extending data association tracking to use multiple detections from multiple detectors, and associated proposal strategies; (7) A new model for the prior on the number of tracks, and associated births and deaths;

and (8) Integrating optical flow and detection information into probabilistic evidence for 3D tracking.

2. Model, priors, and likelihood

In the data-association treatment of the multi-target tracking problem [30, 8], an unknown number of objects (targets) move in a volume, producing observations (detections) at discrete times. The objective is to determine the *association*, ω , which specifies which detections were produced by which target, as well as which were generated spuriously. Here, the targets are the people moving around the ground plane, and the observations (B) are detection boxes obtained by running a person detector [14] on each frame of a video.

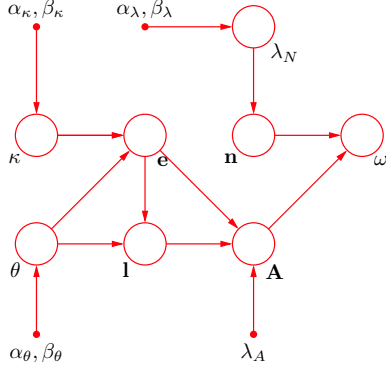
Our goal is to find ω which maximizes the posterior distribution $p(\omega | B) \propto p(B | \omega)p(\omega)$, where $p(\omega)$ is the prior distribution and $p(B | \omega)$ is the likelihood function. The prior over associations contains priors over quantities like the number of tracks and the number of detections per track. The likelihood arises from modeling the underlying 3D scene captured by the video.

In our model, each person in the scene has a 3D configuration \mathbf{z}_r , which is composed of their trajectory (a sequence of points on the ground plane) and their size, which consists of height, width, and girth. We also model evidence from optical flow features [26], I . Using all this, we can compute the likelihood function of an association by integrating out all possible 3D configurations; that is $p(B, I | \omega) = \int p(B | \mathbf{z}, \omega)p(I | \mathbf{z}, \omega)p(\mathbf{z}) d\mathbf{z}$ where the factors in the integrand are, respectively, the two likelihoods of the 3D scene given the two sources of data and the prior over the scene (with $\mathbf{z} = (\mathbf{z}_1, \dots, \mathbf{z}_m)$). The overall graphical model is shown in Figure 1.

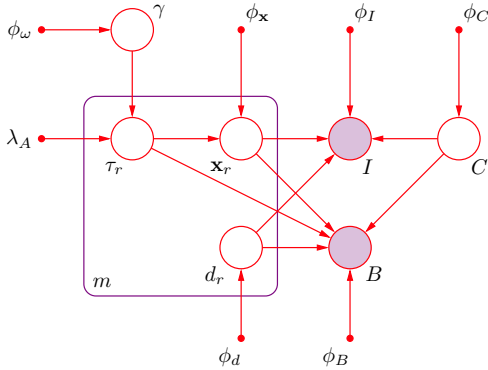
2.1. Association

Formally, an *association* $\omega = \{\tau_r \subset B\}_{r=0}^m$ is a partition of the set of detections B , where τ_1, \dots, τ_m are called *tracks*, and represent across-time chains of observations of the objects being tracked, and τ_0 is the set of false alarms. An example association is shown in Figure 2(a). The association entity is based on well-known work by Oh et al. [31], but we extend that work by (1) allowing tracks to produce multiple measurements at any given frame and (2) employing a prior on associations which allows parameters governing track dynamics and detector behavior to adapt to the environment of a particular video.

We assume an association is the result of the following generative process. When the video starts, there are e_1 people in the scene. At each subsequent frame t , e_t people enter the scene, resulting in $m = \sum_{t=1}^T e_t$ tracks, whose lengths are l_r , $r = 1, \dots, m$. In addition, d_t people exit the scene. At frame t we also observe a_{rt} detections due to person r and n_t detections due to noise. We define $a_t = \sum_{r=1}^m a_{rt}$ as



(a) Graphical model for an association

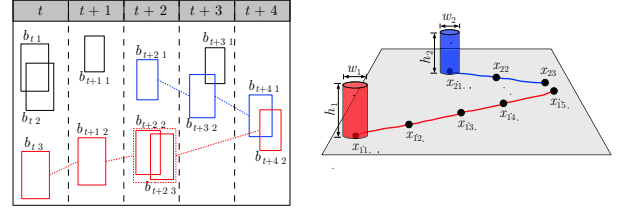


(b) Graphical model after association

Figure 1. Graphical model. Filled circles represent observed variables and red dots represent constants. (a) Graphical model of prior over associations. e , and l are the number of tracks created at each frame and their lengths; n and A are the detections from noise and tracks, respectively; ω is the resulting association. The remaining nodes are parameters for different terms of the prior distribution. (b) Graphical model of the joint distribution, omitting details about the association prior. τ_r are tracks (with $\omega = \{\tau_1, \dots, \tau_m\}$) and $\gamma = (\kappa, \theta, \lambda_N)$ are parameters for the association prior; \mathbf{x}_r denote trajectories, and d_r are the dimensions of objects; C denotes the camera; B is the detection data and I the image optical flow data. The remaining Greek letters (the ϕ s) represent parameters of probability distributions. Noise detections and noise optical flow vectors are omitted.

the number of true detections at frame t , and $N_t = n_t + a_t$ as the total number of detections at t . Finally, a fully-specified assignment in frame t is a permutation of its N_t detections, with the first n_t associated to noise, the next a_{1t} associated to the first track in the frame, etc. (see Figure 1(a))

We assume that $e_1 \sim \mathcal{Pois}(\kappa)$, and that $l_r \sim \mathcal{Exp}(\theta)$, $r = 1, \dots, m$. Assuming the distribution of the number of tracks is stationary, this implies that $e_t \sim \mathcal{Pois}(\kappa\theta)$, $t > 1$. The number of detections per target per frame, as well as the number of noisy detections, are also Poisson distributed, with parameters λ_A and λ_N , respectively. Under these conditions, it can be shown that the prior depends only on the



(a) An example association

(b) Corresponding scene

Figure 2. An example association and its corresponding 3D configuration. (a) An association with two tracks that span a video of five frames. The red boxes make up τ_1 and the blue boxes are τ_2 , while the black boxes are part of the set of false alarms τ_0 . (b) The corresponding 3D scene with two trajectories \mathbf{z}_1 and \mathbf{z}_2 , whose colors correspond to the tracks in (a). Although τ_1 has no detections at time $t + 3$, \mathbf{z}_1 still exists there with position x_{14} .

total tracks m , entrances e , exits d , true detections a , noisy detections n , and track lengths l , as well as the number of ways to permute track labels within frames, and detections within tracks and frames. The resulting expression for $p(\omega | \kappa, \theta, \lambda_N)$ is

$$\frac{(\kappa e^{-\lambda_A})^m \theta^{e+d} \lambda_N^n \lambda_A^a e^{-(\kappa + (T-1)\kappa\theta + l\theta + T\lambda_N)}}{\prod_{t=1}^T (N_t! e_t! n_t! \prod_{i=1}^{m_t} a_{it}!)}, \quad (1)$$

Finally, we consider κ , θ , and λ_N to depend on the video and must infer their values. Consequently, we place vague Gamma priors on them; e.g., $\kappa \sim \mathcal{G}(\alpha_\kappa, \beta_\kappa)$.

2.2. Scene and Camera

Each track $\tau_r \in \omega$, has a corresponding trajectory on the ground plane. The trajectory corresponding to track τ_r is $\mathbf{x}_r = (x_{r1}, \dots, x_{rl_r})^\top$, $x_{rj} \in \mathbb{R}^2$. The length l_r of trajectory \mathbf{x}_r is determined by the first and last detections of track τ_r . Note that, while τ_r contains no elements for frames where the person was not detected, \mathbf{x}_{rj} is specified for every j between the track's initial and final frame. Each person has three size dimensions: width, height and girth, denoted by $d_r = (w_r, h_r, g_r)$. We will denote the 3D configuration of track τ_r by $\mathbf{z}_r = (\mathbf{x}_r, d_r)$.

We model motion as a realization of a multi-output Gaussian process (GP) [33, 35]. Specifically, trajectory \mathbf{x}_r is the curve generated by a sample from a GP with inputs $S_r = \{1, \dots, l_r\}$, with the zero mean function and the squared-exponential covariance function. That is, $\mathbf{x}_r | \tau_r \sim \mathcal{N}(\mathbf{0}, \mathbf{K}_r)$, where \mathbf{K}_r is the covariance matrix, whose element (s, s') is given by $k(s, s') = \sigma_x^2 \exp -\frac{1}{2l_x^2} (s - s')^2$, for all pairs in $S_r \times S_r$. The smoothness and scale parameters l_x and σ_x are set using calibration data. Person size is *a priori* normally distributed, e.g., $h_r \sim \mathcal{N}(\mu_h, \sigma_h)$, following actual human size [27].

Combining these elements and assuming trajectories and sizes to be independent of one another, we get the following

prior for a scene:

$$p(\mathbf{z} | \omega) = \prod_{r=1}^m p(\mathbf{x}_r | \tau_r, \phi_{\mathbf{x}}) p(d_r | \phi_d), \quad (2)$$

where $\phi_{\mathbf{x}} = (l_{\mathbf{x}}, \sigma_{\mathbf{x}})$ and $\phi_d = (\mu_w, \sigma_w, \mu_h, \sigma_h, \mu_g, \sigma_g)$.

Camera. We assume a standard perspective camera [18] with simplifying assumptions[12]. We set the origin of the world to be on the ground plane, for which we use the xz -plane. We assume the camera center to be at $(0, \eta, 0)$ (η is the camera height), a pitch angle of ψ , and a focal length of f (see Figure 3 (top)). Further, we assume the camera has unit aspect ratio, and that the roll, yaw, axis skew, and principal point offset are all zero. We let η , ψ , and f have vague normal priors whose parameters we set manually. Specifically, we have $\eta \sim \mathcal{N}(\mu_\eta, \sigma_\eta)$, $\psi \sim \mathcal{N}(\mu_\psi, \sigma_\psi)$, and $f \sim \mathcal{N}(\mu_f, \sigma_f)$. Assuming independence between parameters, the camera prior is $p(C) = p(\eta | \mu_\eta, \sigma_\eta) p(\psi | \mu_\psi, \sigma_\psi) p(f | \mu_f, \sigma_f)$ where $C = (\eta, \psi, f)$.

Projecting the scene. We convert a 3D scene to a 2D representation by transforming every cylinder at every frame into a 2D box in the image via the camera. Given a trajectory element x_{rj} , we take uniformly-spaced (3D) points on the rims of the cylinder, project them onto the image plane using the camera C and find the minimum bounding box h_{rj} around the resulting 2D points. We call h_{rj} a model box (see Figure 3 (top)).

For each model box h_{rj} , we also compute the region \hat{h}_{rj} that is not occluded from the camera, as follows. First, we discretize h_{rj} into a grid of small cells. We then shoot a ray from the center of each grid cell to the center of the camera, and declare it visible if the ray does not intersect any other box. Then, \hat{h}_{rj} is simply the union of these visible cells.

2.3. Likelihood

We use two sources of evidence: person detectors and optical flow. First, we run various person detectors on the video frames to get bounding boxes $B_t = \{b_{t1}, \dots, b_{tN_t}\}$, $t = 1, \dots, T$, where N_t is the number of detections in frame t . We parametrize each box b_{tj} by $(b_{tj}^x, b_{tj}^{\text{top}}, b_{tj}^{\text{bot}})$, representing the x -coordinate of the center, and the y -coordinates of the top, and bottom, respectively. We also run a dense optical flow estimator on the video, which outputs a set of velocity vectors $I_t = \{v_{t1}, \dots, v_{tN_I}\}$ for each frame $t = 1, \dots, T-1$, where N_I is the number of pixels in the frame. Finally, we use $B = \cup_{t=1}^T B_t$ and $I = \{I_1, \dots, I_{T-1}\}$, and we denote the complete data set by $\mathcal{D} = (B, I)$.

Box likelihood. We model data boxes as having i.i.d. Laplace-distributed errors in the x , top, and bottom parameters. That is, for any assigned data box $b_{tj} \in \tau_r$, $r \neq 0$, and the corresponding model box (for simplicity, assume track τ_r starts at $t = 1$) $h_{rt} = C(x_{rt}, d_r)$, we have

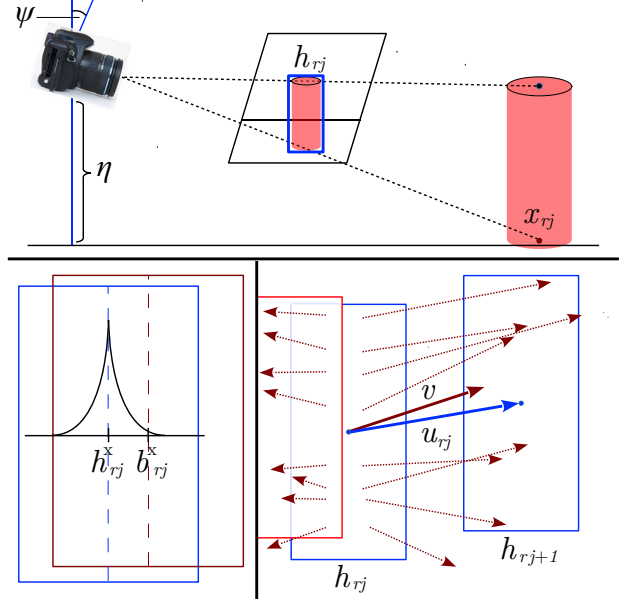


Figure 3. Likelihood computation. Top: the cylinder from target \mathbf{z}_r in frame j gets projected via camera onto the image plane, and model box h_{rj} is computed around it. Bottom-left: The likelihood for the x component of h_{rj} (blue) given one of its corresponding data boxes $b \in B$ (dark red), i.e., $b^x | h_{rj}^x \sim \mathcal{Laplace}(h_{rj}^x, \sigma^x)$. Bottom-right: h_{rj} along with its model direction u_{rj} (thick blue arrow) and the flow vectors it contains (dotted red arrows). The thick red arrow is the average of the flow vectors which lie in \hat{h}_{rj} ; i.e., those not occluded by the red box.

that $b_{tj}^x - h_{rt}^x \sim \mathcal{Laplace}(\mu^x, \sigma^x)$ (see Figure 3 bottom-left) which implies that $b_{tj}^x | h_{rt}^x \sim \mathcal{Laplace}(h_{rt}^x + \mu^x, \sigma^x)$, and analogously for h_{rt}^{top} and h_{rt}^{bot} . At each frame we also observe n_t spurious detections, which we model as uniformly distributed across the image, e.g., $p(b_{tj}^x) = \frac{1}{w_I}$ and $p(b_{tj}^{\text{top}}) = \frac{1}{h_I}$, for all false alarms $b_{tj} \in \tau_0$, where w_I and h_I are the width and height of the image. Combining all these factors, and considering conditional independence, we get a box likelihood $p(B | \mathbf{z}, \omega, C)$ given by

$$\prod_{b \in \tau_0} p(b | w_I, h_I) \prod_{b \in B \setminus \tau_0} p(b | h(b), C, \phi_B), \quad (3)$$

where $h(b)$ is the model box of the cylinder for the target and frame corresponding to box b , and $\phi_B = (\mu^x, \sigma^x, \mu^{\text{top}}, \sigma^{\text{top}}, \mu^{\text{bot}}, \sigma^{\text{bot}})$.

Image likelihood. We aggregate optical flow vector into averages as follows. Let I_B be the set of boxes of all sizes and locations that fit within the image, and $\bar{v}_t(b)$ be the average of the optical flow vectors from frame t contained in box b . We define $I_t = \{\bar{v}_t(b) | b \in I_B\}$, and let $I = \{I_1, \dots, I_{T-1}\}$ as before. Now, consider a pair of consecutive model boxes h_{rt} and $h_{r,t+1}$, and let $u_{rt} = (u_{rt}^x, u_{rt}^y)$ be the difference of their centers (called model direction) and $v = (v^x, v^y) \in I_t$ be the average flow vector that cor-

responds to the box of location and size equal to h_{rt} . We model the error between each of their coordinates as having a Laplace distribution, so that $v^x | u_{rt}^x \sim \mathcal{Laplace}(u_{rt}^x, \sigma_I^x)$, and analogously for v^y (see Figure 3 (bottom-right)). Finally, any $v \in I$ which does not have a corresponding model box has coordinates which have vague Laplace distributions, e.g., $v^x \sim \mathcal{Laplace}(0, \hat{\sigma}_I^x)$.

The full image likelihood $p(I | \mathbf{z}, \omega, C)$ is

$$\prod_{t=1}^{T-1} \left[\prod_{v \in I_t^*} p(v | u(v), C, \phi_I) \prod_{v \in I_t \setminus I_t^*} p(v | \phi_I) \right], \quad (4)$$

where I_t^* is the set of foreground boxes at time t , $u(v)$ is the model direction corresponding to v , and ϕ_I are the Laplace distribution parameters. We can simplify this by taking advantage of the sparsity of the trajectory boxes and dividing by the constant $\prod_{v \in I} p(v | \phi_I)$ to get

$$p(I | \mathbf{z}, \omega, C) \propto \prod_{t=1}^{T-1} \prod_{v \in I_t^*} \frac{p(v | u(v), C, \phi_I)}{p(v | \phi_I)}. \quad (5)$$

Finally, since detection boxes and optical flow are conditionally independent, we have that $p(\mathcal{D} | \mathbf{z}, \omega, C) = p(B | \mathbf{z}, \omega, C)p(I | \mathbf{z}, \omega, C)$

Occlusion. Having a 3D model provides valuable information about occlusion, which we exploit in two ways. In the box likelihood computation, we replace the first factor in eq. 3 with the mixture $|\hat{h}(b)|p(b | h(b), C) + (1 - |\hat{h}(b)|)p(b)$ where $|\hat{h}(b)|$ is the area of $\hat{h}(b)$, i.e., the fraction of $h(b)$ which is visible. In addition, we only average the flow vectors which are contained in the visible cells of the model box which corresponds to $u(v)$ (see figure 3, bottom-right).

3. Inference

We wish to find the MAP estimate of ω as a good solution to the data association problem. In addition, we need to infer the camera parameters C , and the association prior parameters $\gamma = (\kappa, \theta, \lambda_N)$, which we consider functions of the video. Hence, we seek a value (ω, C, γ) that maximizes the posterior distribution

$$p(\omega, C, \gamma | \mathcal{D}) \propto p(\omega | \gamma)p(\gamma)p(C)p(\mathcal{D} | \omega, C) \quad (6)$$

$$= p(\omega | \gamma)p(\kappa)p(\theta)p(\lambda_N)p(C) \quad (7)$$

$$\times \int p(\mathcal{D} | \mathbf{z}, \omega, C)p(\mathbf{z} | \omega) d\mathbf{z},$$

where the factors in the expression are given by equations 1, 2, 3, and 5. To search the space of associations and associated parameters we use Markov chain Monte Carlo (MCMC) sampling techniques. At each iteration, we use different moves to sample over each of three variable blocks, stopping when the posterior stops changing.

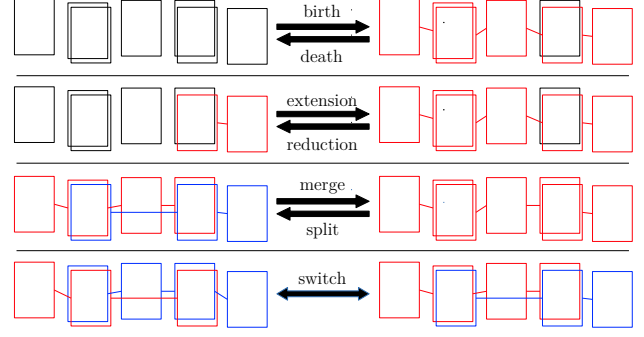


Figure 4. Sampling moves. The blue and red boxes belong to tracks τ_1 and τ_2 , respectively, and the black boxes are part of the false alarms τ_0 .

Sampling association parameters. Sampling γ is straightforward. The full conditional distributions of its components are easy to compute (and sample from), given the conditional independence properties of our model, e.g., $p(\kappa | \theta, \lambda_N, \omega, C, \mathcal{D}) = p(\kappa | \theta, \omega)$, with analogous equalities holding for the full conditionals of θ and λ_N . From this and the conjugate hyper-priors (see Section 2.1), we have that $\kappa | \theta, \omega \sim \mathcal{G}(m + \alpha_\kappa, 1 + (T - 1)\theta + \beta_\kappa)$, $\theta | \kappa, \omega \sim \mathcal{G}(e + d + \alpha_\theta, l + (T - 1)\kappa + \beta_\theta)$, and $\lambda_N | \omega \sim \mathcal{G}(n + \alpha_\lambda, T + \beta_\lambda)$, where the Gamma distribution is parametrized by shape and rate in all cases.

Sampling associations. We use the Metropolis-Hastings (MH) algorithm to sample from $p(\omega | \gamma, C, \mathcal{D})$, using an extension of the MCMCDA proposal mechanism [31, 8]. Let ω be the current sample. We draw an association ω' from the proposal distribution $q(\cdot | \omega)$, which we accept or reject based on the MH acceptance probability

$$\min \left(1, \frac{p(\omega' | \gamma, C, \mathcal{D})q(\omega | \omega')}{p(\omega | \gamma, C, \mathcal{D})q(\omega' | \omega)} \right). \quad (8)$$

We use seven sampling moves to efficiently explore the space of associations, which are loosely based on the standard MCMCDA moves. At each MH iteration, we perform move j with probability $q_m(j)$, where $j \in \{1, \dots, 7\}$, (birth is 1, death 2, etc.). In what follows, let $\omega = \{\tau_0, \dots, \tau_m\}$ be the current sample, and ω' be the proposed association.

Birth/death moves. A frame, t_i , is sampled uniformly, and the first detection $\tau_{m'+1}$ in the new-born track $\tau_{m'}$ is sampled uniformly from the set of false alarms at time t_i . We then decide whether to grow forward or backward in time with probability $\frac{1}{2}$. Assuming forward growth: to grow to time $t = t_i + 1$, we fit a line through the bottom of the previous s boxes, extrapolate the position of the next box, and independently choose to append candidates at time t based on their squared distance from the predicted point (see Figure 5). If none of the detections from time t is assigned, we stop growing $\tau_{m'}$ with probability c ; otherwise, we continue with $t + 1$. The new association is then set to

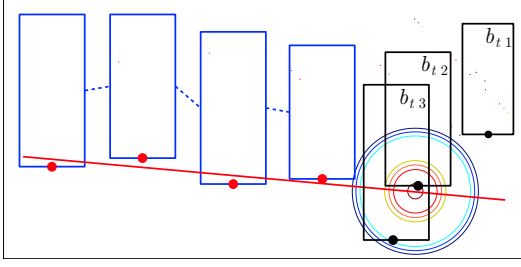


Figure 5. The growing procedure and the disconnect move. The blue boxes represent the last detections of the track, the red line is fit to their bottoms and extrapolates the ideal position of the new boxes, represented by the center of the concentric circles. The black boxes are then appended to the track based on their distance from the ideal point (e.g., in this case, $b_{t,2}$ has the best chance of being added).

be $\omega' = \omega \cup \{\tau_{m'}\}$. To kill a track, we choose r uniformly from $\{1 \dots, m\}$, and let $\omega' = \omega \setminus \{\tau_r\}$.

Extension/reduction moves. For extension, we choose a track τ_r uniformly. We then grow it forward or backward to produce $\tau_{r'}$ using the procedure described for the birth move. For reduction, we pick a detection $\tau_{r,j}$ uniformly from $\{\tau_{r,2}, \dots, \tau_{r,l_r-1}\}$, choose a direction, and remove all detections from the track after (or before) $\tau_{r,j}$. In both, the resulting association is $\omega' = (\omega \setminus \{\tau_r\}) \cup \{\tau_{r'}\}$.

Merge/split moves. We replace the standard MCMCDA merge and split moves with alternatives that exploit the fact that we allow tracks to contain multiple detections from a single frame. In the merge move, we assign a weight to each pair of tracks $(\tau_{r'}, \tau_{r''})$ proportional to the probability of birthing track $\tau_{r'} \cup \tau_{r''}$, as described in the birth move above. We then choose a pair based on those probabilities, and the resulting track becomes $\tau_r = \tau_{r'} \cup \tau_{r''}$. The proposed association then becomes $\omega' = (\omega \setminus \{\tau_{r'}, \tau_{r''}\}) \cup \tau_r$. To split track τ_r , we first choose two frames t and t' uniformly, $t < t'$. All detections before t go to $\tau_{r'}$, and all detections after t' go to $\tau_{r''}$. Each detection between t and t' go to either track with probability $\frac{1}{2}$. The resulting association is $\omega' = (\omega \setminus \{\tau_r\}) \cup \{\tau_{r'}, \tau_{r''}\}$.

Switch move. First select tracks r_1 and r_2 uniformly, and choose one detection from each track (with indices j and k) such that their locations are within a distance \bar{v} times their temporal offset. Then, the detections after j in track r_1 and those before k in track r_2 are swapped. The proposed association is $\omega' = (\omega \setminus \{\tau_{r_1}, \tau_{r_2}\}) \cup \{\tau'_{r_1}, \tau'_{r_2}\}$.

Once we sample ω' , we must evaluate its posterior (eq. 7), which contains an integral over \mathbf{z} that corresponds to the marginal likelihood of ω' . Due to the camera projection, this likelihood cannot be performed analytically, nor can it be computed numerically, due to the high dimensionality of \mathbf{z} . Instead, we estimate the value of the integral using the Laplace-Metropolis approximation [17], which uses the fact that

$p(\mathcal{D} | \omega, C) = p(\mathcal{D} | \mathbf{z}^*, \omega, C)p(\mathbf{z}^* | \omega) / p(\mathbf{z}^* | \mathcal{D}, \omega, C)$, where $\mathbf{z}^* = \arg \max p(\mathcal{D} | \mathbf{z}, \omega, C)p(\mathbf{z} | \omega)$. If we approximate the denominator with the Gaussian pdf, we get

$$p(\mathcal{D} | \omega, C) \approx (2\pi)^{\frac{D}{2}} |\mathbf{H}|^{-\frac{1}{2}} p(\mathcal{D} | \mathbf{z}^*, \omega, C)p(\mathbf{z}^* | \omega), \quad (9)$$

where \mathbf{H} is the Hessian of $-\log(p(\mathcal{D} | \mathbf{z}, \omega, C)p(\mathbf{z} | \omega))$ evaluated at \mathbf{z}^* , and D is the dimension of \mathbf{z} .

We estimate \mathbf{z}^* using the Hybrid Monte Carlo (HMC) algorithm [29], using central finite differences to approximate the gradient of the posterior $p(\mathbf{z} | \mathcal{D}, \omega, C)$. We also use finite differences to approximate \mathbf{H} at \mathbf{z}^* . Unfortunately, the finite differences approximation requires too many evaluations of the posterior, an expensive calculation. To address this, we exploit the conditional independence that exists between frames in the likelihood, e.g., $p(b, b' | \mathbf{z}, \omega, C) = p(b | \mathbf{z}, \omega, C)p(b' | \mathbf{z}, \omega, C)$, in two ways. In the gradient computation, for example, updating a single dimension of \mathbf{z} only affects a small number of boxes, whose likelihoods we can update independently of the rest. Conditional independence also means that most off-diagonal elements of \mathbf{H} are very close to 0, a fact which we exploit by only computing the finite differences on the diagonal.

Sampling cameras. We use HMC to sample from the camera posterior $p(C | \gamma, \omega, B, I) \propto p(B, I | C, \omega)p(C)$, as this has proved effective in the task of camera estimation under a similar parametrization [12]. We use the same HMC implementation as that used to approximate \mathbf{z}^* for eq. 9.

4. Data preparation and calibration

Data. For person detections, we used the readily available MATLAB implementation of the object detector developed by Felzenszwalb et al. [14], pre-trained for humans. We found that the detector missed well-defined smaller figures, mitigated by using double-sized images. For image data, we precomputed the dense optical flow of each frame using an existing software [26]. To speed up the computation of the average flow (§2.3), we precompute the integral flow of each frame using integral images.

Parameter calibration. We manually annotated boxes for 47 videos from the *DARPA Mind's Eye Year One (ME-Y1)* data set.¹, by drawing tight bounding boxes around each target throughout the video. To calibrate relevant parameters of the generative model, we match each detection box to the ground truth box with which it has maximum overlapping area, provided it is greater than 50%, otherwise it is counted as a false detection. Using this matching, we find reasonable values for λ_A and for the parameters of the likelihoods ϕ_B and ϕ_I . For the former, we simply average number of detections associated to each ground truth box; we estimate the latter using a maximum likelihood approach

¹<http://www.visint.org/datasets>

(using the ground truth boxes). The remaining parameters are set manually.

Initialization. The sampler is initialized with an empty association ($\omega = \{\}$), and a camera C which is fit to the data B under the box likelihood (eq. 3) using RANSAC [15].

5. Experiments and results

We tested our tracker on two widely-used data sets: the *PETS 2009* data set², and the *TUD* data set³. For *PETS* we tested on the *S2L1* video, which has over 795 frames, and contains 19 pedestrians walking freely about a very large area. The *TUD* data set contains three videos, called *campus*, *crossing*, and *Stadtmitte*, with 71, 201, and 179 frames, respectively, featuring between 8 and 13 people walking across the screen, and which were taken with a very low camera angle, causing targets to be frequently occluded for long periods of time.

Performance measures. We use the CLEAR metrics [38] which consists of two measurements, multiple object tracking accuracy (MOTA) and multiple object tracking precision (MOTP). MOTA is a measure of false positives, missed targets and track switches, and ranges from $-\infty$ to 1, with 1 being a perfect score. MOTP measures the average distance between true and inferred trajectories, and ranges from 0 to the threshold at which tracks are said to correspond which, as per convention, we set to 1 meter.

We also use the evaluation proposed by Li et al. [25], of which we are using two metrics: mostly tracked (MT) and mostly lost (ML). We use a threshold of 80% for declaring a target mostly tracked.

Experiments. We report the results of running our tracker on *PETS* and *TUD*, as well as published results for other algorithms in Table 1. We also ran experiments designed to test the impact of the different parts of our model, in which we ran our tracker with certain aspects disabled. Here we used the relatively easy *TUD-Campus* video. The results for these experiments are in Table 2. Not surprisingly, the performance took the greatest blow when the tracker ignored optical flow features. These results also suggest that our handling of occlusion is also quite helpful, which supports our fully 3D approach.

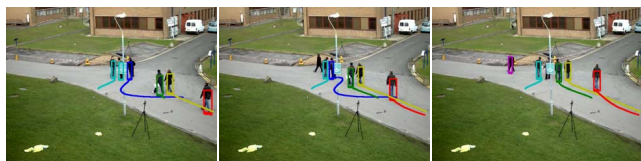


Figure 6. Visualization of some of our results: three frames of the *PETS-S2L1* video with the 3D scene super-imposed.

²<http://www.cvg.rdg.ac.uk/PETS2009/a.html>

³<https://www.d2.mpi-inf.mpg.de/node/382>

	Method	MOTA	MOTP	MT	ML
<i>PETS</i>	Our method	0.83	0.8	0.67	0
	Zamir [34]	0.9	×	×	×
	Wu [41]	0.88	×	0.87	0.05
	Andriyenko [5]	0.96	0.78	0.96	0
	Andriyenko [2]	0.88	0.76	0.87	0.05
<i>TUD-X</i>	Our method	0.80	0.78	0.69	0.08
	Zamir [34]	0.91	×	×	×
<i>TUD-S</i>	Our method	0.70	0.73	0.7	0
	Zamir [34]	0.78	×	×	×
	Andriyenko [5]	0.62	0.63	0.67	0
	Andriyenko [4]	0.60	0.66	0.67	0
	Andriyenko [2]	0.68	0.65	0.55	0
<i>TUD-C</i>	Our method	0.84	0.81	0.75	0.25
	Yan [42]	0.85	×	×	×

Table 1. Comparison of performance of our approach and several state-of-the-art algorithms on the *PETS* and *TUD* (*campus*, *crossing*, and *Stadtmitte*, labeled *TUD-C*, *TUD-X*, *TUD-S*, resp.) data sets using the CLEAR metrics, as well as those proposed in [25]. We report MOTP as normalized distance, and use × for values not reported, or reported in 2D.

Method	MOTA	MOTP	MT	ML
Base	0.84	0.81	0.75	0.25
NO-OF	0.59	0.79	0.38	0.25
NO-OCC	0.73	0.81	0.62	0.25

Table 2. A summary of the effect of removing key features of our tracker. “Base” is our full algorithm, “NO-OF” ignores optical flow features, and NO-OCC does not reason about occlusion.

6. Discussion

We presented a tracker which incorporates representations for data association and 3D scene in a principled way. Across all data sets and all measures our method is comparable to the state-of-the-art. Since our approach is Bayesian and expandable, we expect performance will improve as it matures. In addition, our algorithm is easily parallelizable. We emphasize that we are learning more about the scene than other approaches typically do. In particular, we infer the camera and sizes of the tracked persons. We expect that further modeling improvements will similarly lead to better tracking and inferring more about the scene.

7. Acknowledgments

This material is based upon work supported in part by the DARPA Mind’s Eye program, and by the National Science Foundation under Grant No. IIS-0747511.

References

- [1] M. Andriluka, S. Roth, and B. Schiele. Monocular 3d pose estimation and tracking by detection. In *CVPR*, pages 623–630, 2010. 1
- [2] A. Andriyenko, S. Roth, and K. Schindler. An analytical formulation of global occlusion reasoning for multi-target tracking. In *ICCV Workshop*, pages 1839–1846, 2011. 7

- [3] A. Andriyenko and K. Schindler. Globally optimal multi-target tracking on a hexagonal lattice. In *ECCV*, pages 466–479, 2010. **2**
- [4] A. Andriyenko and K. Schindler. Multi-target tracking by continuous energy minimization. In *CVPR*, 2011. **1, 2, 7**
- [5] A. Andriyenko, K. Schindler, and S. Roth. Discrete-continuous optimization for multi-target tracking. In *CVPR*, pages 1926–1933, 2012. **1, 2, 7**
- [6] B. Benfold and I. Reid. Stable multi-target tracking in real-time surveillance video. In *CVPR*, pages 3457–3464, 2011. **1**
- [7] M. Betke, D. E. Hirsh, A. Bagchi, N. I. Hristov, N. C. Makris, and T. H. Kunz. Tracking large variable numbers of objects in clutter. In *CVPR*, 2007. **2**
- [8] E. Brau, K. Barnard, R. Palanivelu, D. Dunatunga, T. Tsukamoto, and P. Lee. A generative statistical model for tracking multiple smooth trajectories. In *CVPR*, pages 1137–1144, 2011. **2, 5**
- [9] P. Carr, Y. Sheikh, and I. Matthews. Monocular object detection using 3d geometric primitives. In *ECCV*, pages 864–878, Berlin, Heidelberg, 2012. Springer-Verlag. **2**
- [10] W. Choi and S. Savarese. Multiple target tracking in world coordinate with single, minimally calibrated camera. *ECCV*, pages 553–567, 2010. **2**
- [11] K. Choo and D. Fleet. People tracking with hybrid monte carlo. *ICCV*, II:321–328, 2001. **2**
- [12] L. Del Pero, J. Guan, E. Brau, J. Schlecht, and K. Barnard. Sampling bedrooms. *CVPR*, pages 2009–2016, 2011. **4, 6**
- [13] A. Ess, B. Leibe, K. Schindler, and L. van Gool. Robust multiperson tracking from a mobile platform. *IEEE PAMI*, 31(10):1831–1846, October 2009. **2**
- [14] P. Felzenszwalb, R. Girshick, D. McAllester, and D. Ramanan. Object detection with discriminatively trained part-based models. *IEEE PAMI*, 2009. **2, 6**
- [15] M. A. Fischler and R. C. Bolles. Random sample consensus: A paradigm for model fitting with applications to image analysis and automated cartography. *Comm. of the ACM*, 24:381–395, 1981. **7**
- [16] F. Fleuret, J. Berclaz, R. Lengagne, and P. Fua. Multi-camera people tracking with a probabilistic occupancy map. *IEEE PAMI*, 2007. **2**
- [17] W. Gilks, S. Richardson, and D. Spiegelhalter. Introducing markov chain monte carlo. In W. Gilks, S. Richardson, and D. Spiegelhalte, editors, *Markov chain Monte Carlo in practice*. Chapman and Hall, 1996. **6**
- [18] R. Hartley and A. Zisserman. *Multiple View Geometry in Computer Vision*. Cambridge University Press, 2000. **4**
- [19] D. Hoiem, A. A. Efros, and M. Hebert. Putting objects in perspective. In *CVPR*, 2006. **2**
- [20] M. Isard and A. Blake. Condensation – conditional density propagation for visual tracking. *Int. J. Comp. Vis.*, 29(1):5–28, 1998. **1**
- [21] M. Isard and J. MacCormick. Bramble: A bayesian multiple-blob tracker. In *ICCV*, pages 34–41, 2001. **2**
- [22] Z. Khan, T. Balch, and F. Dellaert. Mcmc-based particle filtering for tracking a variable number of interacting targets. *PAMI*, 27(11):1805–1819, 2005. **1**
- [23] C. Kuo, C. Huang, and R. Nevatia. Multi-target tracking by on-line learned discriminative appearance models. In *CVPR*, pages 685–692, 2010. **1**
- [24] S. Kwak, W. Nam, B. Han, and J. H. Han. Learning occlusion with likelihoods for visual tracking. *ICCV*, 2011. **1**
- [25] Y. Li, C. Huang, and R. Nevatia. Learning to associate: Hybridboosted multi-target tracker for crowded scene. *CVPR*, 2000. **7**
- [26] C. Liu. *Exploring New Representations and Applications for Motion Analysis*. PhD thesis, M.I.T., 2009. **2, 6**
- [27] M. A. McDowell, C. D. Fryar, R. Hirsch, and C. L. Ogden. Anthropometric reference data for children and adults: U.s. population, 1999–2002. *Advance Data*, (361), July 2005. **3**
- [28] R. Mohedano and N. Garcia. Simultaneous 3d object tracking and camera parameter estimation by bayesian methods and transdimensional mcmc sampling. In *ICIP*, 2011. **2**
- [29] R. M. Neal. Probabilistic inference using markov chain monte carlo methods. Technical report, 1993. **6**
- [30] S. Oh. Bayesian formulation of data association and markov chain monte carlo data association. In *Robotics: Science and Systems Conference (RSS) Workshop Inside Data association*, 2008. **2**
- [31] S. Oh, S. Russell, and S. Sastry. Markov chain Monte Carlo data association for general multiple target tracking problems. 2004. **1, 2, 5**
- [32] K. Okuma, A. Taleghani, N. d. Freitas, J. Little, and D. Lowe. A boosted particle filter: Multitarget detection and tracking. In *ECCV*, 2004. **1**
- [33] C. E. Rasmussen and C. K. I. Williams. *Gaussian Processes For Machine Learning*. MIT Press, 2006. **3**
- [34] A. Roshan Zamir, A. Dehghan, and M. Shah. Gmcp-tracker: Global multi-object tracking using generalized minimum clique graphs. In *ECCV*, pages 343–356. 2012. **7**
- [35] M. Seeger. Gaussian processes for machine learning. *Int. J. of Neural Systems*, 14(2):69–106, 2004. **3**
- [36] H. Sidenbladh, M. Black, and D. Fleet. Stochastic tracking of 3d human figures using 2d image motion. *ECCV*, II:702–718, 2000. **2**
- [37] C. Sminchisescu and B. Triggs. Kinematic jump processes for monocular 3d human tracking. In *CVPR*, 2003. **2**
- [38] R. Stiefelhagen, K. Bernardin, R. Bowers, J. Garofolo, D. Mostefa, and P. Soundararajan. The clear 2006 evaluation. In *Proceedings of the 1st international evaluation conference on Classification of events, activities and relationships*, CLEAR’06, pages 1–44, Berlin, Heidelberg, 2007. **7**
- [39] C. Wojek, S. Roth, K. Schindler, and B. Schiele. Monocular 3d scene modeling and inference: Understanding multi-object traffic scenes. *ECCV*, pages 467–481, 2010. **1, 2**
- [40] Z. Wu, T. H. Kunz, and M. Betke. Efficient track linking methods for track graphs using network-flow and set-cover techniques. *CVPR*, pages 1185–1192, 2011. **2**
- [41] Z. Wu, A. Thangali, S. Sclaroff, and M. Betke. Coupling detection and data association for multiple object tracking. *CVPR*, pages 1948–1955, June 2012. **1, 7**
- [42] X. Yan, X. Wu, I. A. Kakadiaris, and S. K. Shah. To track or to detect? an ensemble framework for optimal selection. In *ECCV*, pages 594–607, 2012. **7**